



Published in final edited form as:

*Pain*. 2014 December ; 155(12): 2646–2655. doi:10.1016/j.pain.2014.09.030.

## Fast Conducting Mechanoreceptors Contribute to Withdrawal Behavior in Normal and Nerve Injured Rats

M. Danilo Boada<sup>a</sup>, Thomas J. Martin<sup>a</sup>, Christopher M. Peters<sup>a</sup>, Kenichiro Hayashida<sup>a</sup>, Michael H. Harris<sup>a</sup>, Timothy T. Houle<sup>a</sup>, Edward S. Boyden<sup>b</sup>, James C. Eisenach<sup>a</sup>, and Douglas G. Ririe<sup>a</sup>

<sup>a</sup>Department of Anesthesiology, Wake Forest School of Medicine, Winston-Salem, North Carolina, USA

<sup>b</sup>The Synthetic Neurobiology Group, Media Lab, Massachusetts Institute of Technology, Cambridge, Massachusetts, USA

### Abstract

Fast conducting myelinated high threshold mechanoreceptors (AHTMR) are largely thought to transmit acute nociception from the periphery. However, their roles in normal withdrawal and in nerve injury induced hyperalgesia are less well accepted. Modulation of this subpopulation of peripheral neurons would help define their roles in withdrawal behaviors. The optically active proton pump, ArchT, was placed in an AAV8 viral vector with the CAG promoter and was administered by intrathecal injection resulting in expression in myelinated neurons. Optical inhibition of peripheral neurons at the soma and transcutaneously was possible in the neurons

© 2014 Elsevier B.V. on behalf of International Association for the Study of Pain. All rights reserved.

Address correspondence to: Douglas G. Ririe, MD, PhD, Department of Anesthesiology, Wake Forest School of Medicine, Medical Center Boulevard, Winston-Salem, NC 27157-1009, Ph: 336-716-4498, Fax: 336-716-8190, dririe@wakehealth.edu.

**Contributions:** M. Danilo Boada: Conception and design of research, performed experiments, analyzed data, interpreted results, prepared figures, drafted, edited, revised and approved final version manuscript.

Thomas J. Martin: Conception and design of research, interpreted results, edited, revised and approved final version manuscript.

Christopher M. Peters: Design of research, performed experiments, analyzed data, interpreted results, prepared figures, drafted, edited, revised and approved final version manuscript.

Kenichiro Hayashida: Performed experiments, edited, revised and approved final version manuscript.

Timothy T. Houle: Design of research, analyzed data, interpreted results, edited, revised and approved final version manuscript.

Edward S. Boyden: Conception and design of research, interpreted results, edited, revised and approved final version manuscript.

James C. Eisenach: Conception and design of research, interpreted results, edited, revised and approved final version manuscript.

Douglas G. Ririe: Conception and design of research, performed experiments, analyzed data, interpreted results, prepared figures, drafted, edited, revised and approved final version manuscript.

**Competing Financial Interests:** M. Danilo Boada: None.

Thomas J. Martin: None.

Christopher M. Peters: None.

Kenichiro Hayashida: None.

Timothy T. Houle: None.

Edward S. Boyden: Patents: ArchT, Methods and compositions for decreasing chronic pain. Co-founder: Eos Neuroscience. Consultant: GSK, 3scan, Medtronic, Center for Technology Advancement.

James C. Eisenach: Patent: Methods and compositions for decreasing chronic pain. Consultant: Adynxx, Aerial Biopharm

Douglas G. Ririe: Patent: Methods and compositions for decreasing chronic pain.

**Publisher's Disclaimer:** This is a PDF file of an unedited manuscript that has been accepted for publication. As a service to our customers we are providing this early version of the manuscript. The manuscript will undergo copyediting, typesetting, and review of the resulting proof before it is published in its final citable form. Please note that during the production process errors may be discovered which could affect the content, and all legal disclaimers that apply to the journal pertain.

expressing ArchT, but not in neurons from control animals. Receptive field characteristics and electrophysiology determined that inhibition was neuronal subtype specific with only AHTMR neurons being inhibited. One week following nerve injury the AHTMR are hyperexcitable, but can still be inhibited at the soma and transcutaneously. Withdrawal thresholds to mechanical stimuli in normal and in hyperalgesic nerve injured animals were also increased by transcutaneous light to the affected hindpaw. This suggests that AHTMR neurons play a role not only in threshold related withdrawal behavior in the normal animal, but also in sensitized states after nerve injury. This is the first time this subpopulation of neurons has been reversibly modulated to test their contribution to withdrawal related behaviors before and after nerve injury. This technique may prove useful to define the role of selective neuronal populations in different pain states.

## Keywords

A fiber; C fiber; Electrophysiology; Hyperalgesia; Mechanotransduction; Nerve injury; Neuropathic, Nociceptor, Optogenetics; Pain; Sensory neuron; Withdrawal

## 1.0 Introduction

“First” pain or acute pain has been attributed to fast conducting, myelinated A- $\delta$  fibers, while persistent types of pathologic pain have been attributed to slow conducting, unmyelinated C-fibers [20,26]. Selective reduction or ablation shows convincingly that C-fibers contribute to various pain states, yet their ablation does not entirely eliminate pain behavior [9,44]. This suggests other peripheral nerves contribute to ongoing nociception, likely A- $\delta$  or A- $\beta$  neurons. However, the contribution of A-fiber subsets has been largely inferred due to lack of selective ablation or modulation techniques. Contributing to the limited understanding of A-fibers is the fact that no biomarker distinguishes the subsets of myelinated fibers.

Although conduction velocity (CV) has long been used to classify peripheral neurons, CV alone is an artificial characterization of nerve sensibility. Therefore, further classification of neurons is performed using receptive field (RF) properties. Mechanically activated nociceptors have CVs in the C-fiber and A-fiber range, are responsible for noxious stimulus detection, and respond to various stimuli [31,51]. These mechanically sensitive neurons are high threshold, but after injury they may become sensitized [18,51]. In this study, we have focused on neurons classified as fast conducting, myelinated (A- $\delta$  fiber), nociceptive high threshold mechanoreceptors (AHTMR) [4,38] that are distinguished from non-nociceptive, or tactile, low threshold mechanoreceptors (LTMR). The AHTMRs have long been considered “first” pain fibers, but their contribution to normal responses from suprathreshold input, ongoing abnormal input, and responses following nerve injury are not well appreciated [20,26,31].

Inhibition of a subset of myelinated neurons using the powerful molecular tools available to control neuronal activity would permit probing their role in normal and neuropathic conditions [2,5,11,35,54,57]. Optically active channels and pumps are one such tool and hold promise for therapeutic application and interrogation of cellular systems [3,8,11,19,29,36]. Although this requires both targeted gene delivery/expression and light

delivery, advances to increase light sensitivity and tissue specificity and delivery have been important for studying neuronal connections in the brain [3,11,12,14,15,23,28,32,37,50,58].

Circuitry and modulation of the spinal cord or peripheral nervous system receive less attention than the brain [8,17,24,25,33,43,49,52]. Spinal cord studies using optogenetics have largely focused on motor neurons and circuits [33,49], with recent effort targeting spinal cord sensory circuitry and peripheral sensory input and pain [8,17,24,25]. Optically active molecules to activate and inhibit nociception and pain behavior in peripheral nerves has been reported [17,24,25]. Selectively targeting subpopulations of nociceptive neurons and the possibility of transcutaneous activation of channels may result in advancement of this technology in pain related studies. In this study we used an optically active proton pump, ArchT, for neuronal transduction, expression and modulation (Fig. 1). We hypothesized that normal peripheral afferent neurons could be inhibited optically *in vitro* and *in vivo* [13]. We further hypothesized that activity in hyperexcitable neurons from nerve injury could be reduced. Selective inhibition of a subtype of nociceptive neurons, AHTMR, was an unanticipated finding demonstrated by selective expression in A-fibers and electrophysiologic confirmation of isolated AHTMR modulation which has permitted the investigation of AHTMR in the withdrawal related behavior in normal and nerve injured animals.

## 2.0 Methods

### 2.1 Viral vector administration and expression of ArchT-GFP

All studies were approved by the Wake Forest University Institutional Animal Care and Use Committee (ACUC) and adhere to the guidelines of the Committee for Research and Ethical Issues of IASP. Male Sprague-Dawley rats were used for all studies (weight range for injection 100-150g, Harlan Laboratories, Indianapolis, IN). Replication deficient AAV8/CAG-ArchT-GFP or AAV8/CAG-GFP control constructs were obtained from the Boyden Laboratory (The Synthetic Neurobiology Group, Media Lab, Massachusetts Institute of Technology, Cambridge, Massachusetts, USA; ArchT plasmid and map available at Addgene 29777) and the viral vectors produced by the Vector Core Facility at the University of North Carolina at Chapel Hill, USA. Three different manufactured lots of viral vector were used. Ten  $\mu$ L of replication deficient AAV8 vector containing ArchT with a GFP tag (no stop codon between the ArchT and GFP) and a CAG promoter or control vector containing CAG and GFP only ( $1 \times 10^{12}$  viral particles/ml) was injected at the level of the L4-5 spinous processes in male Sprague-Dawley rats under brief isoflurane anesthetic using a 30 g needle. Tail flick was used for confirmation of needle placement. Animals were not randomized to treatment. All animals showed expression after presumed intrathecal injection. For expression, 1-, 2- 4-, 8-, and 12-weeks after injection, animals (N=4 at each time point) were euthanized with pentobarbital and perfused with 4% paraformaldehyde in 0.1M phosphate buffered saline (PBS), DRG isolated, cryoprotected in 30% sucrose in 0.1M PBS, frozen sectioned at 16  $\mu$ m, and visualized using fluorescent microscopy. GFP visualization was performed without enhancement when possible. When used with other fluorophores GFP was visualized using standard immunohistochemical methods. GFP visualization in DRG, nerve roots and spinal cord (spinal cord 35  $\mu$ m sections) was

performed using a Nikon epifluorescence microscope without antibody enhancement of the GFP using frozen sections in 50% ethanol and cover slipped. Multi-labelling DRG imaging was performed 4 weeks after injection. In this case, the sections were incubated for 60 min at room temperature in a blocking solution of 3% normal donkey serum in 0.1M PBS with 0.3% Triton X-100 and then incubated overnight at 4°C with primary antibodies. Myelinated primary afferent sensory nerve fibers were labeled with a mouse monoclonal anti-200Kd neurofilament antibody (NF200, 1:1000; Serotec, Raleigh, NC). Viral vector transduced cells were visualized with a rabbit polyclonal anti-green fluorescent protein antibody (GFP, 1:5000; Abcam, Cambridge, UK). Unmyelinated IB4 positive cells were stained with IB4-biotin (1:2000; Sigma-Aldrich, St. Louis, MO). Sections were then washed in PBS and incubated for 3 h at RT with appropriate secondary antibodies conjugated to fluorescent markers (CY3 1: 600, Cy2 1:400 and streptavidin conjugated Cy5 1:2000, respectively; Jackson ImmunoResearch, West Grove, PA). Finally, DRG sections were washed, dehydrated, cleared, and cover-slipped images captured using a Nikon epifluorescence microscope. DRG co-labelled for GFAP and GFP were processed in a similar fashion using the rabbit polyclonal anti-GFP antibody (1:5000; Abcam, Cambridge, UK) and mouse polyclonal anti-GFAP (1:1000; Sigma-Aldrich, St. Louis, MO). Sections were then washed in PBS and incubated for 3 h at RT with secondary antibodies conjugated to fluorescent markers (Cy2 1:400 and Cy3 1:600, respectively; Jackson ImmunoResearch, West Grove, PA). Glabrous skin of the hindpaw was prepared in a similar fashion after pSNL. Sensory nerve fibers were labeled with a pan neuronal marker polyclonal rabbit anti-PGP 9.5 antibody (1:4000; Ultracone, Cambridge, UK; Catalog number RA95101). Myelinated primary afferent sensory nerve fibers were labeled with a mouse monoclonal anti-200Kd neurofilament antibody (NF200, 1:1000; Serotec, Raleigh, NC). Viral vector transduced cells were visualized with a chicken polyclonal anti-GFP antibody (1:1000; Invitrogen, Grand Island, NY). Sections were then washed in PBS and incubated for 3 h at RT with secondary antibodies conjugated to fluorescent markers (CY5 1: 500, Cy3 1:600 and Cy2 1:400, respectively; Jackson ImmunoResearch, West Grove, PA). Finally, skin sections were washed, dehydrated, cleared, and cover-slipped images were captured using a confocal microscope. Co-labelling of DRG for GFAP and GFP was performed in 16 micron cryosectioned DRG.

## 2.2 *In vitro* intracellular recording from DRG

Four weeks after injection, animals (n=12) were euthanized and the L4 DRG removed and placed in a chamber and mounted on the stage of an upright microscope (BX50-WI; Olympus America, Inc., Center Valley, PA), continuously perfused with oxygenated artificial cerebrospinal fluid (aCSF) containing 130 mM NaCl, 3.5 mM KCl, 1.25 mM NaH<sub>2</sub>PO<sub>4</sub>, 24 mM NaHCO<sub>3</sub>, 10 mM dextrose, 1.2 mM MgCl<sub>2</sub>, and 1.2 mM CaCl<sub>2</sub> (pH = 7.3) at a rate of 2 ml/min, and the temperature was maintained at 37±1°C as described previously [41].

DRG neurons were visualized under differential interference contrast through a digital camera and intracellular electrophysiologic recordings were obtained with a sharp microelectrode filled with 2.5 M potassium acetate (pH = 7.2) (Supplemental Fig. 2b). Satisfactory recordings were obtained with electrodes of 50–80 MΩ. The electrophysiologic

data were collected with the use of a single-electrode continuous current clamp (AxoClamp-2B; Axon Instruments, Foster City, CA) and analyzed with Clampex 8 software (Axon Instruments).

After a stabilization period of 10 min, a neuron containing GFP was isolated. Acceptable neurons had a resting membrane potential ( $E_m$ ) < -45 millivolts (mV) and a peak action potential (AP) height greater than 0 mV regardless of the  $E_m$ , i.e., overshoot of the AP height over 0 mV. After a period of stabilization of the  $E_m$  of approximately 3 min, a current clamp protocol was begun. The current clamp protocol consisted of depolarizing currents of 0.1–4.0 nanoamperes (nA) (100-ms pulse duration) delivered in increments of 0.1 nA until an AP was evoked (Supplemental Fig. 2c). The threshold current (rheobase (Rh)) was defined as the minimum current required to evoke an AP. From each DRG, 1–2 cells were studied.  $E_m$  was first measured 3 min after a stable recording was obtained and was measured again after the end of the protocol.  $E_m$  and Rh were measured before, after light exposure for 2 min and 5 min (Irradiance= 0.013 mW/mm<sup>2</sup>) and after the light was off. Light power density was calculated per unit area after measuring the light energy in mW using an analog power meter (Thorlabs, Inc., Newton, NJ).

**2.2.1 *In vivo* Studies**—Three to 8 weeks after intrathecal ArchT injection male Sprague-Dawley rats were deeply anesthetized (isoflurane), monitored, artificially ventilated (tracheotomy), and immobilized (pancuronium) as described previously [4]. A laminectomy was performed exposing L4 DRG ganglia. The surface of the ganglia was superfused with oxygenated aCSF. The spinal column was secured using custom clamps and the animal was transferred to a preheated (32–34°C) recording chamber where the superfusate was slowly raised to 37°C (MPRE8; Cell MicroControls, Norfolk, VA). Pool temperature adjacent to the DRG was monitored with a small thermocouple (IT-23; Physitemp, Clifton, NJ). Rectal temperature (RET-3; Physitemp) was maintained at 34±1°C with radiant heat. Intracellular records were obtained with borosilicate microelectrodes (80–250 MΩ) containing 1 M potassium acetate and further analyses were done on cells with identified RFs. RFs were searched with a fine sable-hair brush to locate the peripheral RF. For afferents requiring higher intensities, subsequent searches used increasingly stiffer probes and finally sharp-tipped forceps. Afferents with cutaneous RFs were distinguished from those with deep RFs by displacing skin to ensure that RFs would track with the skin rather than remain stationary. Mechanical thresholds (MTs) were characterized with calibrated von Frey filaments (Stoelting, Wood Dale, IL).

Intracellular penetrations with a resting membrane potential of  $\leq -35$  mV were characterized further. DC output was digitized and analyzed off-line using Spike2 (CED, Cambridge, UK). Sampling rate for intracellular recordings was 21 kHz throughout (MicroPower1401; CED). Passive (e.g.,  $R_i$ ,  $\tau$ , Rh) and active properties were measured. CV was measured by the application of electrical stimulation on the cellular skin RF at the lowest current intensity required to evoke an AP. Any neuron with jitter was rejected. Stimuli ranged in duration from 50–100  $\mu$ s; utilization time was not taken into account. Conduction distances were measured for each afferent on termination of the experiment by inserting a pin through the RF (marked with ink at the time of recording) and carefully measuring the distance to the DRG along the closest nerve. Afferent classification using 12 parameters was used for

mechanosensitive neurons to follow standard definitions based on response to mechanical stimuli, CV, and adaptation rate and active and passive membrane properties as previously described [4]. All included cells satisfied the following requirements: resting membrane potential more negative than -30 mV, AP amplitude  $\geq 30$  mV, and the presence of spike AHP. Passive membrane properties indicative of poor impalement were also reason for exclusion. Mechanosensitive neurons were classified as LTMR, AHTMR or C-fiber high threshold mechanoreceptor (CHTMR) based on CV, electrophysiologic profile and RF properties as previously described [4].

To determine the effects of light on the cellular responses, a laser of wavelength 532 nm (Irradiance 0.03-0.34 mW/mm<sup>2</sup>) (Shanghai Laser & Optics Century Co., Ltd., Shanghai, China) was focused on the L4 DRG soma to determine the neuronal effects of activation of the ArchT channel directly at the cellular membrane. Transcutaneous illumination of ArchT was performed by focusing the laser on the glabrous surface of the paw in the RF where peripheral testing was being performed. The cellular electrical properties and its responsiveness were also tested under these conditions.

### 2.3 Behavioral Mechanical Stimulation Testing

Animals were placed on a mesh surface in a plastic cage and were acclimated for 20 min before testing. Withdrawal to mechanical stimulation was assessed with the hind paws resting on the mesh surface and application of calibrated von Frey filaments to the plantar surface of the foot until the filaments bent. This was done 3 times, with a positive response determined by brisk withdrawal of the paw. The force in grams resulting in withdrawal with a 50% probability was determined using the up-down method as previously described [4,41]. The von Frey filaments used were 3.84, 4.08, 4.31, 4.56, 4.74, 4.93, 5.18, 5.46, 5.88, 6.10, and 6.45, corresponding to 0.5, 0.9, 1.7, 3.7, 5.5, 8.0, 12.4, 21.5, 53.0, 72.0, and 129 g. Withdrawal thresholds were determined before pSNL, after pSNL at 2 weeks, and with light for 2 min and without light focused in the hindpaw RF where the von Frey filaments were being tested. Response was determined by a person blinded to treatment. All animals were included in the data analysis, and no animal in the study had a wound dehiscence or infection during the study.

### 2.4 Partial Spinal Nerve Ligation

The animals were deeply anesthetized with isoflurane and under aseptic conditions the skin was incised at the midline over the lumbar spine. The right L5 spinal nerve was identified and approximately 1/3 thickness of the L5 spinal nerve was ligated with 9-0 nylon suture under the dissecting microscope [22]. Care was taken not to pull the nerve or contact the intact L4 spinal nerve. After hemostasis was achieved, the muscle layer was approximated with 4-0 synthetic absorbable suture (Look, Reading, PA) and the skin closed with absorbable suture. In a sham control group, the surgical procedure was identical to that described above, except that the right L5 spinal nerve was not injured. After the surgery, the rats were returned to their cages, kept warm under a heat lamp, and monitored during recovery.



## 2.5 Statistical analysis

All data were analyzed for normal distribution. Data are presented as means and standard deviations. Power analysis was performed only for the change in withdrawal threshold after nerve injury to detect a difference in MWT of 5 grams using a power of 0.8 and an alpha of 0.05 with a standard deviation of 5 to yield a sample size of 8. Statistical significance was tested using one-way and two-way ANOVA, repeated measures ANOVA, or the paired *t*-test. Correction for multiple comparisons was performed when appropriate. For comparison of proportion of fibers, a Chi-square test or Fisher's exact test was used where appropriate. Analysis was performed with SAS 9.2. By convention, a two-tailed test was used and  $p < 0.05$  was considered significant for all analyses.

## 3.0 Results

### 3.1 Neuronal expression after intrathecal administration

ArchT transduction in peripheral neurons using an AAV8-CAG-ArchT-GFP viral vector construct and IT administration resulted in expression in dorsal root ganglia (DRG) neuronal soma and in axons and dendrites (Fig 2a). The peak expression (N=4 animals at each time point) was approximately 10% of soma and was achieved between 2-4 weeks after injection and remained stable beyond 12 weeks (Fig. 2b and Supplemental Fig 1a). Only peripheral sensory neurons were transduced while astrocytes, motor and spinal cord neurons and satellite cells in DRG were completely spared (Supplemental Fig. 1b,c). The GFP-ArchT protein is transported antidromically and orthodromically from the soma (Fig. 1a). GFP is present in sensory axons entering the dorsal medial spinal cord (Supplemental Fig. 1c) and in nerve terminals in the skin 4 weeks after IT administration (Supplemental Fig. 1d). Expression of ArchT was restricted to myelinated neurons (>98% of GFP positive cells were NF200 positive cells) with <1% of GFP positive cells expressing IB4 and 27% of myelinated cells were GFP positive (Fig. 2c,d).

### 3.2 Functional neuronal electrophysiology

After *in vivo* administration, ArchT was functionally active using *in vitro* single cell electrophysiology in DRG neurons (n=12 neurons from 12 DRG from 12 animals). Supplemental Fig. 2a,b,c) [41]. Light activation of ArchT produced hyperpolarization (decreased resting membrane potential ( $E_m$ )) and reduced excitability (increased rheobase ( $R_h$ )) at 2 minutes of light (Irradiance= 0.013 mW/mm<sup>2</sup>)(Fig. 3a,b). After 5 min of light, no action potential (AP) was generated in 4/12 cells at 2×  $R_h$  (Supplemental Fig. 2c). The effects fully resolved after the light was off. Light produced no change in  $R_h$  or  $E_m$  in any cell from control animals (n=12 neurons from 12 DRG from 12 animals).

*In vivo* DRG electrophysiology (Fig. 4a,b) showed that only myelinated, fast-conducting (A-type fiber), high-threshold mechanoreceptors (AHTMR) (Supplemental Fig. 2d) were affected by light with resulting hyperpolarization, while the myelinated, fast conducting (A-type fiber), low-threshold mechanoreceptors (LTMR) and the unmyelinated, slow-conducting (C-type fiber), high-threshold mechanoreceptors (CHTMR) were unchanged (Fig. 1g) ( $p < 0.05$ ) [4]. Neuronal responses from electrical somatic activation and suprathreshold RF activation were inhibited using somatically focused laser light at a

wavelength of 532 nm (Irradiance 0.03-0.1 mW/mm<sup>2</sup>)(Fig. 4c,d). Blinded subtype-selective neuronal somatic inhibitory effects of the light were tested in 82 cells after peripheral nerve RF activation (N=49 cells (maximum one neuron of each type per animal) from 20 animals containing ArchT vector and N=33 cells from 8 animals with control vector). DRG laser illumination inhibited 15/15 AHTMR neurons tested while no LTMR (0/19) or CHTMR (0/15) neuron exhibited any change in firing rate in the ArchT containing DRG ( $p < 0.0001$ ). In the control vector containing DRG, no cell of any type could be inhibited by DRG laser illumination (0/8 AHTMR; 0/17 LTMR; 0/8 CHTMR). Finally, transcutaneous efficacy of light inhibition in the RF was tested using intracellular *in vivo* electrophysiology at the soma (Irradiance 0.03-0.5 mW/mm<sup>2</sup>)(N=23 DRG neurons (maximum one neuron of each type per animal) from 11 animals) (Fig. 5 a-d). All AHTMR (8/8) neurons could be inhibited, while none of the CHTMR (0/7) and LTMR (0/8) neurons was inhibited ( $p < 0.0001$ ). AHTMRs were readily inhibited at threshold (Fig. 5b) and at suprathreshold and the response to light was intensity-dependent using instantaneous frequency of the neuronal AP responses (Fig. 5c,d).

### 3.3 Neuronal control after nerve injury

Sensory afferents become hyperexcitable following injury and may drive chronic pain. However, reducing activity following injury may be different from the basal state. Therefore neurons were made hyperexcitable using nerve injury to test for inhibition. Two weeks following partial sciatic nerve ligation (pSNL) (ligation of the L5 nerve root, Fig. 6a) AHTMR neurons in the L4 DRG were hyperexcitable with decreased mechanical thresholds (MT), increased APs to a given stimulus, increased RF size, and displayed after depolarizations following stimuli ( $p < 0.05$ ) (Fig. 6a,b,c,d) [22]. AHTMR MTs were reduced by pSNL as were mechanical withdrawal thresholds (MWT) in freely behaving animals (N=28 AHTMR neurons from 11 pSNL and 17 sham/control) (Fig. 6c). IT administration of AAV8-ArchT 1 week prior to pSNL permitted inhibition of AHTMR (9/9 cells)(N=9 animals) neurons 2 weeks after pSNL with transcutaneous light (Irradiance 0.03-0.1 mW/mm<sup>2</sup>) rendering the RF insensitive to high-threshold stimuli, suprathreshold von Frey stimulus, or pinch. However, CHTMR (0/6) and LTMR (0/7) neurons could not be inhibited with transcutaneous light (Fig. 6e). No difference in mechanical withdrawal thresholds was found over time after injection of viral vector relative to control in the absence of light (N=16 animals; 8 viral vector and 8 control) (Supplemental Fig. 3a). Transcutaneous light administered with a laser (Irradiance 0.15-0.34 mW/mm<sup>2</sup>) increased MWT in normal (N=8) (Supplemental Fig. 3b) and nerve-injured animals after ArchT(N=8) ( $p < 0.05$ ) and MWT returned to baseline after stopping light (Fig. 6d). No change in MWT in response to light was observed in controls (N=8) or pSNL animals with no ArchT (N=8).

## 4.0 Discussion

This is the first report of inhibition of peripheral neurons in rat after IT administration of an ArchT AAV construct. The data corroborate previous reports that *in vitro* and *in vivo* inhibition of sensory input from the periphery can be achieved using optically active proteins [24]. Moreover, we present data on functional transduction of ArchT in a subset of mechanosensitive neurons, AHTMRs. Although these fibers have long been established as



nociceptors, selective control made it possible to directly establish their contribution to mechanical withdrawal behavior in the rat under normal conditions and in a model of neuropathic pain using a rapidly reversible and non-pharmacologic manipulation [7,31].

In this study, we have focused on mechanically sensitive and fast conducting peripheral nerve fibers and their contributions to withdrawal behavior. These fast conducting mechanoreceptors, or AHTMRs, are considered “first” pain fibers, or acute nociceptors [20,26,31]. While the contribution of these fibers to “first” pain signaling is accepted, their role in normal and nerve injury is unclear. Our data suggest that they contribute to normal responses from suprathreshold input, ongoing abnormal input, and responses following nerve injury; first by demonstrating a correlation between withdrawal threshold and AHTMR sensibility, then by demonstrating increased sensibility of the AHTMR after nerve injury, and finally demonstrating that inhibition of transmission results in altered behavioral withdrawal responses under normal and pathologic conditions.

Nerve injury induced pain is often generated by normally innocuous stimuli, associated with enhanced responses to noxious stimuli, and may be elicited in the absence of activation within the RF [1,16]. These responses can persist long after the initial injury, spread to uninjured areas and may reflect changes in neighboring neurons or DRG that innervate areas within or in proximity to areas innervated by damaged nerves. In this study we focused on the uninjured L4 DRG, which is also abnormal after L5 injury. Hypersensitivity and allodynia are important contributors to nerve injury pain, and withdrawal thresholds in animals are commonly used to assess this [6,10]. The A-fibers from within the injured nerves are thought to contribute to spontaneous pain [27]. However, differential effects of nerve injury on injured and intact nerves may give rise to different components of pain, in particular elicited versus spontaneous pain [18,42,55]. Increased sensibility of intact A-fibers after nerve injury has recently been reported [18]. Our data corroborate these findings that A-fibers in the uninjured DRG are sensitized after injury. However, no spontaneous activity was observed in any neuron in our study before or after injury consistent with other reports [45]. We extend these findings by demonstrating that A-fibers are not just A- $\delta$  fibers, but AHTMR and move from speculation that the lowered A-nociceptor thresholds and sensitization may contribute to greater evoked pain to a definitive link between the A nociceptor sensitization and reduced withdrawal thresholds, considered pain related behavior, by reducing pain related behavior with optical inhibition of the AHTMR in a reversible manner.

The widest classification of peripheral neurons is based on CV, but many modalities are used. The contribution of peripheral nerve subtypes to different sensations is confounded in part because classification based on physiologic or anatomic characteristics do not accurately reflect the precise identity of the nerve under study. Ideally the availability of a biomarker, genetic or protein, would permit definitive identification of neuronal subtypes and be valuable in understanding the contribution of neuronal subsets to varying pathologic and non-pathologic behavioral responses. RF characteristics are one way of accurately identifying a nerve, but these methods are cumbersome. Definitive identification of neurons without the need to arduously characterize the RF response characteristics would be advantageous, especially since the RF is not readily available with in vitro preps and non-

existent in culture. Subtype selective markers have been identified for some neurons, but the ability to distinguish mechanically sensitive afferents based on biologic markers remains a major obstacle. Most progress in this area is in distinguishing A- from C- fibers or separate subtypes of C-fibers. Subclassification of C-fibers is based on IB4 immunoreactivity or on presence of peptidergic expression [34,48], but even this is not entirely reliable with large species variability [39]. More specific identification of subsets of unmyelinated neurons has been reported [9]. Myelinated neurons can be distinguished in the rat by the presence of specific neurofilaments [30]. However, further subclassification of myelinated neurons that reliably distinguish and divide them based on RF characteristics as well as CV, adaptation rate and electrical properties is not available. Specific biomarkers which contribute to the neuronal RF characteristics would contribute significantly to understanding the mechanisms of neuronal selectivity of the viral vector/promoter and be valuable for development of tools for selective activation and inhibition of other neuronal subtypes. Since peptidergic markers are in both myelinated and IB4 positive neurons, the particular AHTMR population defined by expression in this study is likely not confined to a particular peptidergic marker. The fact that >98% of the GFP positive neurons are myelinated suggests the effects on withdrawal are not significantly derived from C-fibers. Nevertheless, further studies to determine the identity of AHTMR neurons immunohistochemically in a more comprehensive fashion will be useful.

This is the first study to demonstrate functional transduction of a subset of myelinated neurons with a protein construct using a viral vector. IT administration was chosen due to technical ease, routine clinical use, and previous reports with successful transduction [47]. Other methods have been utilized; intraneural injection, injection into the DRG, localized injection relying on retrograde transport, and systemic injection [21,24,46,47,53,56]. AAV8 seems to have affinity for peripheral nerves even after muscle or systemic administration [21,56]. Selectivity of AAV8 constructs for sensory fibers after IT injection has been demonstrated [47], but no selectivity for AHTMR neurons has been reported. In our case, preferential expression in myelinated neurons may play a role, but would not explain the lack of expression in motor neurons. Expression of specific glycoproteins on myelinated sensory neurons which permit AAV8 greater binding and possibly improved access is a possible explanation. Also serotype differences in properties of capsid may alter genome release during cell entry influencing cell type and tissue specificity [40]. Studies of AAV8 mechanisms of cell entry and selectivity will enhance utility of AAV8 in the periphery and IT space. In our studies, no gross evidence of cellular damage or toxicity was found either *in vitro* or *in vivo*; however, we did not specifically study this aspect of expression and further testing is required to adequately assess the risks beyond laboratory investigations.

The precise control of channels in a neuronal subtype specific fashion opens the possibility of therapeutic intervention utilizing light, possibly patient controlled, for spatial and temporal control of afferent nociceptive input to control pain. This would provide a novel treatment approach for pain syndromes. However, optogenetic applications are currently limited to animals, but advances in gene therapy and light devices combined with the use of transcutaneous light could open the door for clinical application of this technology for treatment of pain [11,12,14,23,32,50]. Reduction of nociceptive input while maintaining

light touch and motor function and simultaneously avoiding CNS depressive effects of commonly used drug therapy would be desirable. Clinical translation would be enhanced by the efficacy of transcutaneous light which can be easily controlled in a temporal, spatial and wavelength specific fashion [2,5,13,14]. This would eliminate the need for implantation of an illuminating device. However, skin thickness and access of nerve endings to light may be a limitation of transcutaneous activation in larger animals or humans. Further testing to define the applicability and limitations of transcutaneous efficacy will be essential. Understanding the mechanisms of neuronal specificity will be critical for further translation of this technology to other species and ultimately to humans. In the meantime, the powerful use of selective optical inhibition of peripheral nociceptive input as a tool should yield valuable knowledge about different pain states that have been difficult to study with the currently available methods.

Together these data demonstrate that the peripheral sensory nervous system can be targeted and controlled with light-activated inhibitory pumps. Our data from a neuropathic pain model demonstrate that sensory neuron subtype control permits interrogation of pain-related changes in processing sensory information and can advance knowledge of spinal circuits that modulate and transmit nociceptive input from peripheral sensory nerves [26]. In particular, ArchT is promising as a tool to assess the AHTMR contribution to peripheral pain states [14]. Further targeting of other neuronal subtypes will enhance understanding of spinal cord circuitry and the contribution of other sensory subtypes to peripheral nociception and their role in the generation and maintenance of various peripherally driven pain states. Finally, our data support the complexity of the ubiquitous withdrawal behavior in the rat, suggest contributions from different peripheral neurons and establish a role of AHTMR activity in withdrawal behavior in normal rats and after nerve injury.

## Supplementary Material

Refer to Web version on PubMed Central for supplementary material.

## Acknowledgments

We would like to thank Renee Parker, Tanishua Bynum and Addie Larimore for technical assistance and Joseph Tobin, MD for support and discussions. We also would like to recognize Alan Horsager, PhD of Eos Neuroscience, Inc. and Kenneth Greenberg, PhD of Spiral Genomics, Inc. for discussions. We would also like to thank Dr. R. Jude Samulski and the University of North Carolina Viral Core facility. This work was supported by the Department of Anesthesiology and the National Institutes of Health GM48085 to JCE and GM104249 to DGR. Neither the funding sponsor had any role in the design, conduct, analysis and interpretation of the study, nor were they involved in the writing or decision to submit the manuscript for publication.

## References

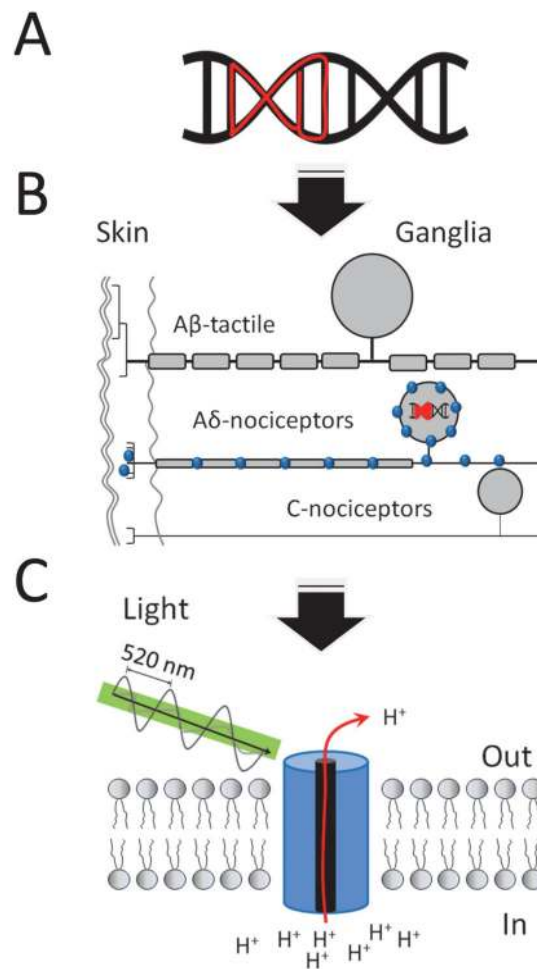
1. Basbaum AI, Bautista DM, Scherrer G, Julius D. Cellular and molecular mechanisms of pain. *Cell*. 2009; 139:267–84. [PubMed: 19837031]
2. Bernstein JG, Boyden ES. Optogenetic tools for analyzing the neural circuits of behavior. *Trends Cogn Sci*. 2011; 15:592–600. [PubMed: 22055387]
3. Beyeler A, Eckhardt CA, Tye KM. Deciphering memory function with optogenetics. *Prog Mol Biol Transl Sci*. 2014; 122:341–90. [PubMed: 24484707]

4. Boada MD, Houle TT, Eisenach JC, Ririe DG. Differing neurophysiologic mechanosensory input from glabrous and hairy skin in juvenile rats. *J Neurophysiol.* 2010; 104:3568–75. [PubMed: 20926608]
5. Boyden ES, Zhang F, Bamberg E, Nagel G, Deisseroth K. Millisecond-timescale, genetically targeted optical control of neural activity. *Nat Neurosci.* 2005; 8:1263–8. [PubMed: 16116447]
6. Bridges D, Thompson SW, Rice AS. Mechanisms of neuropathic pain. *Br J Anaesth.* 2001; 87:12–26. [PubMed: 11460801]
7. Burgess PR, Perl ER. Myelinated afferent fibres responding specifically to noxious stimulation of the skin. *J Physiol.* 1967; 190:541–62. [PubMed: 6051786]
8. Carr FB, Zachariou V. Nociception and pain: lessons from optogenetics. *Front Behav Neurosci.* 2014; 8:69. [PubMed: 24723861]
9. Cavanaugh DJ, Lee H, Lo L, Shields SD, Zylka MJ, Basbaum AI, Anderson DJ. Distinct subsets of unmyelinated primary sensory fibers mediate behavioral responses to noxious thermal and mechanical stimuli. *Proc Natl Acad Sci U S A.* 2009; 106:9075–80. [PubMed: 19451647]
10. Chaplan SR, Bach FW, Pogrel JW, Chung JM, Yaksh TL. Quantitative assessment of tactile allodynia in the rat paw. *J Neurosci Methods.* 1994; 53:55–63. [PubMed: 7990513]
11. Chow BY, Boyden ES. Optogenetics and translational medicine. *Sci Transl Med.* 2013; 5:177ps5.
12. Chow BY, Boyden ES. Physiology. Synthetic physiology. *Science.* 2011; 332:1508–9. [PubMed: 21700858]
13. Chow BY, Han X, Boyden ES. Genetically encoded molecular tools for light-driven silencing of targeted neurons. *Prog Brain Res.* 2012; 196:49–61. [PubMed: 22341320]
14. Chow BY, Han X, Dobry AS, Qian X, Chuong AS, Li M, Henninger MA, Belfort GM, Lin Y, Monahan PE, Boyden ES. High-performance genetically targetable optical neural silencing by light-driven proton pumps. *Nature.* 2010; 463:98–102. [PubMed: 20054397]
15. Chuong AS, Miri ML, Busskamp V, Matthews GAC, Acker LC, Soresnsen AT, Young A, Klapoetke NC, Henninger MA, Kodandaramaiah SB, Ogawa M, Ramanlal SB, Bandler RC, Allen BD, Forest CR, Chow BY, Han X, Lin Y, Tye KM, Roska R, Cardin JA, Boyden ES. Non-invasive optical inhibition with a red-shifted microbial rhodopsin. *Nature Neuroscience.* 2014 In Press.
16. Costigan M, Scholz J, Woolf CJ. Neuropathic pain: a maladaptive response of the nervous system to damage. *Annu Rev Neurosci.* 2009; 32:1–32. [PubMed: 19400724]
17. Daou I, Tuttle AH, Longo G, Wieskopf JS, Bonin RP, Ase AR, Wood JN, De Koninck Y, Ribeiro-da-Silva A, Mogil JS, Séguéla P. Remote optogenetic activation and sensitization of pain pathways in freely moving mice. *J Neurosci.* 2013; 33:18631–40. [PubMed: 24259584]
18. Djouhri L, Fang X, Koutsikou S, Lawson SN. Partial nerve injury induces electrophysiological changes in conducting (uninjured) nociceptive and non-nociceptive DRG neurons: Possible relationships to aspects of peripheral neuropathic pain and paresthesias. *Pain.* 2012; 153:1824–36. [PubMed: 22721911]
19. Doroudchi MM, Greenberg KP, Liu J, Silka KA, Boyden ES, Lockridge JA, Arman AC, Janani R, Boye SE, Boye SL, Gordon GM, Matteo BC, Sampath AP, Hauswirth WW, Horsager A. Virally delivered channelrhodopsin-2 safely and effectively restores visual function in multiple mouse models of blindness. *Mol Ther.* 2011; 19:1220–9. [PubMed: 21505421]
20. Dworkin RH. An overview of neuropathic pain: syndromes, symptoms, signs, and several mechanisms. *Clin J Pain.* 2002; 18:343–9. [PubMed: 12441827]
21. Foust KD, Poirier A, Pacak CA, Mandel RJ, Flotte TR. Neonatal intraperitoneal or intravenous injections of recombinant adeno-associated virus type 8 transduce dorsal root ganglia and lower motor neurons. *Hum Gene Ther.* 2008; 19:61–70. [PubMed: 18052722]
22. Guan Y, Yuan F, Carteret AF, Raja SN. A partial L5 spinal nerve ligation induces a limited prolongation of mechanical allodynia in rats: an efficient model for studying mechanisms of neuropathic pain. *Neurosci Lett.* 2010; 471:43–7. [PubMed: 20067820]
23. Han X, Chow BY, Zhou H, Klapoetke NC, Chuong A, Rajimehr R, Yang A, Baratta MV, Winkle J, Desimone R, Boyden ES. A high-light sensitivity optical neural silencer: development and application to optogenetic control of non-human primate cortex. *Front Syst Neurosci.* 2011; 5:18. [PubMed: 21811444]

24. Iyer SM, Montgomery KL, Towne C, Lee SY, Ramakrishnan C, Deisseroth K, Delp SL. Virally mediated optogenetic excitation and inhibition of pain in freely moving nontransgenic mice. *Nat Biotechnol.* 2014; 32:274–8. [PubMed: 24531797]
25. Ji ZG, Ito S, Honjoh T, Ohta H, Ishizuka T, Fukazawa Y, Yawo H. Light-evoked somatosensory perception of transgenic rats that express channelrhodopsin-2 in dorsal root ganglion cells. *PLoS One.* 2012; 7:e32699. [PubMed: 22412908]
26. Julius D, Basbaum AI. Molecular mechanisms of nociception. *Nature.* 2001; 413:203–10. [PubMed: 11557989]
27. Kajander KC, Bennett GJ. Onset of a painful peripheral neuropathy in rat: a partial and differential deafferentation and spontaneous discharge in A- $\beta$  and A- $\delta$  primary afferent neurons. *J Neurophysiol.* 1992; 68:734–44. [PubMed: 1331353]
28. Klapoetke NC, Murata Y, Kim SS, Pulver SR, Birdsey-Benson A, Cho YK, Morimoto TK, Chuong AS, Carpenter EJ, Tian Z, Wang J, Xie Y, Yan Z, Zhang Y, Chow BY, Surek B, Melkonian M, Jayaraman V, Constantine-Paton M, Wong GK, Boyden ES. Independent optical excitation of distinct neural populations. *Nat Methods.* 2014; 11:338–46. [PubMed: 24509633]
29. Kokaia M, Sørensen AT. The treatment of neurological diseases under a new light: the importance of optogenetics. *Drugs Today (Barc).* 2011; 47:53–62. [PubMed: 21373649]
30. Lawson SN, Waddell PJ. Soma neurofilament immunoreactivity is related to cell size and fibre conduction velocity in rat primary sensory neurons. *J Physiol.* 1991; 435:41–63. [PubMed: 1770443]
31. Lewis TT, Pochin EE. The double pain response of the human skin to a single stimulus. *Clin Sci.* 1937; 3:67–76.
32. Lin JY, Lin MZ, Steinbach P, Tsien RY. Characterization of engineered channelrhodopsin variants with improved properties and kinetics. *Biophys J.* 2009; 96:1803–14. [PubMed: 19254539]
33. Llewellyn ME, Thompson KR, Deisseroth K, Delp SL. Orderly recruitment of motor units under optical control in vivo. *Nat Med.* 2010; 16:1161–5. [PubMed: 20871612]
34. McCarthy PW, Lawson SN. Differing action potential shapes in rat dorsal root ganglion neurones related to their substance P and calcitonin gene-related peptide immunoreactivity. *J Comp Neurol.* 1997; 388:541–9. [PubMed: 9388014]
35. Nichols CD, Roth BL. Engineered G-protein coupled receptors are powerful tools to investigate biological processes and behaviors. *Front Mol Neurosci.* 2009; 2:16. [PubMed: 19893765]
36. Pama EA, Colzato LS, Hommel B. Optogenetics as a neuromodulation tool in cognitive neuroscience. *Front Psychol.* 2013; 4:610. [PubMed: 24046763]
37. Papagiakoumou E. Optical developments for optogenetics. *Biol Cell.* 2013; 105:443–64. [PubMed: 23782010]
38. Perl ER. Myelinated afferent fibres innervating the primate skin and their response to noxious stimuli. *J Physiol.* 1968; 197:593–615. [PubMed: 4969883]
39. Price TJ, Flores CM. Critical evaluation of the colocalization between calcitonin gene-related peptide, substance P, transient receptor potential vanilloid subfamily type 1 immunoreactivities, and isolectin B4 binding in primary afferent neurons of the rat and mouse. *J Pain.* 2007; 8:263–72. [PubMed: 17113352]
40. Rayaprolu V, Kruse S, Kant R, Venkatakrishnan B, Movahed N, Brooke D, Lins B, Bennett A, Potter T, McKenna R, Agbandje-McKenna M, Bothner B. Comparative analysis of adeno-associated virus capsid stability and dynamics. *J Virol.* 2013; 87:13150–60. [PubMed: 24067976]
41. Ririe DG, Liu B, Clayton B, Tong C, Eisenach JC. Electrophysiologic characteristics of large neurons in dorsal root ganglia during development and after hind paw incision in the rat. *Anesthesiology.* 2008; 109:111–7. [PubMed: 18580180]
42. Sapunar D, Ljubkovic M, Lirk P, McCallum JB, Hogan QH. Distinct membrane effects of spinal nerve ligation on injured and adjacent dorsal root ganglion neurons in rats. *Anesthesiology.* 2005; 103:360–76. [PubMed: 16052119]
43. Sharp AA, Fromherz S. Optogenetic regulation of leg movement in midstage chick embryos through peripheral nerve stimulation. *J Neurophysiol.* 2011; 106:2776–82. [PubMed: 21880945]

44. Shields SD, Cavanaugh DJ, Lee H, Anderson DJ, Basbaum AI. Pain behavior in the formalin test persists after ablation of the great majority of C-fiber nociceptors. *Pain*. 2010; 151:422–9. [PubMed: 20832171]
45. Smith AK, O'Hara CL, Stucky CL. Mechanical sensitization of cutaneous sensory fibers in the spared nerve injury mouse model. *Mol Pain*. 2013; 9:61. [PubMed: 24286165]
46. Storek B, Harder NM, Banck MS, Wang C, McCarty DM, Janssen WG, Morrison JH, Walsh CE, Beutler AS. Intrathecal long-term gene expression by self-complementary adeno-associated virus type 1 suitable for chronic pain studies in rats. *Mol Pain*. 2006; 2:4. [PubMed: 16445862]
47. Storek B, Reinhardt M, Wang C, Janssen WG, Harder NM, Banck MS, Morrison JH, Beutler AS. Sensory neuron targeting by self-complementary AAV8 via lumbar puncture for chronic pain. *Proc Natl Acad Sci U S A*. 2008; 105:1055–60. [PubMed: 18215993]
48. Stucky CL, Lewin GR. Isolectin B(4)-positive and -negative nociceptors are functionally distinct. *J Neurosci*. 1999; 19:6497–505. [PubMed: 10414978]
49. Towne C, Montgomery KL, Iyer SM, Deisseroth K, Delp SL. Optogenetic control of targeted peripheral axons in freely moving animals. *PLoS One*. 2013; 8:e72691. [PubMed: 23991144]
50. Wentz CT, Bernstein JG, Monahan P, Guerra A, Rodriguez A, Boyden ES. A wirelessly powered and controlled device for optical neural control of freely-behaving animals. *J Neural Eng*. 2011; 8:046021. [PubMed: 21701058]
51. Woolf CJ, Ma Q. Nociceptors--noxious stimulus detectors. *Neuron*. 2007; 55:353–64. [PubMed: 17678850]
52. Wyart C, Del Bene F, Warp E, Scott EK, Trauner D, Baier H, Isacoff EY. Optogenetic dissection of a behavioural module in the vertebrate spinal cord. *Nature*. 2009; 461:407–10. [PubMed: 19759620]
53. Yu H, Fischer G, Ferhatovic L, Fan F, Light AR, Weihrauch D, Sapunar D, Nakai H, Park F, Hogan QH. Intraganglionic AAV6 results in efficient and long-term gene transfer to peripheral sensory nervous system in adult rats. *PLoS One*. 2013; 8:e61266. [PubMed: 23613824]
54. Zalocusky K, Deisseroth K. Optogenetics in the behaving rat: integration of diverse new technologies in a vital animal model. *Optogenetics*. 2013; 1:1–17.
55. Zhang XF, Zhu CZ, Thimmapaya R, Choi WS, Honore P, Scott VE, Kroeger PE, Sullivan JP, Faltynek CR, Gopalakrishnan M, Shieh CC. Differential action potentials and firing patterns in injured and uninjured small dorsal root ganglion neurons after nerve injury. *Brain Res*. 2004; 1009:147–58. [PubMed: 15120592]
56. Zheng H, Qiao C, Wang CH, Li J, Li J, Yuan Z, Zhang C, Xiao X. Efficient retrograde transport of adeno-associated virus type 8 to spinal cord and dorsal root ganglion after vector delivery in muscle. *Hum Gene Ther*. 2010; 21:87–97. [PubMed: 19719401]
57. Zhu H, Roth BL. Silencing synapses with DREADDs. *Neuron*. 2014; 82:723–5. [PubMed: 24853931]
58. Zorzos AN, Boyden ES, Fonstad CG. Multiwaveguide implantable probe for light delivery to sets of distributed brain targets. *Opt Lett*. 2010; 35:4133–5. [PubMed: 21165114]

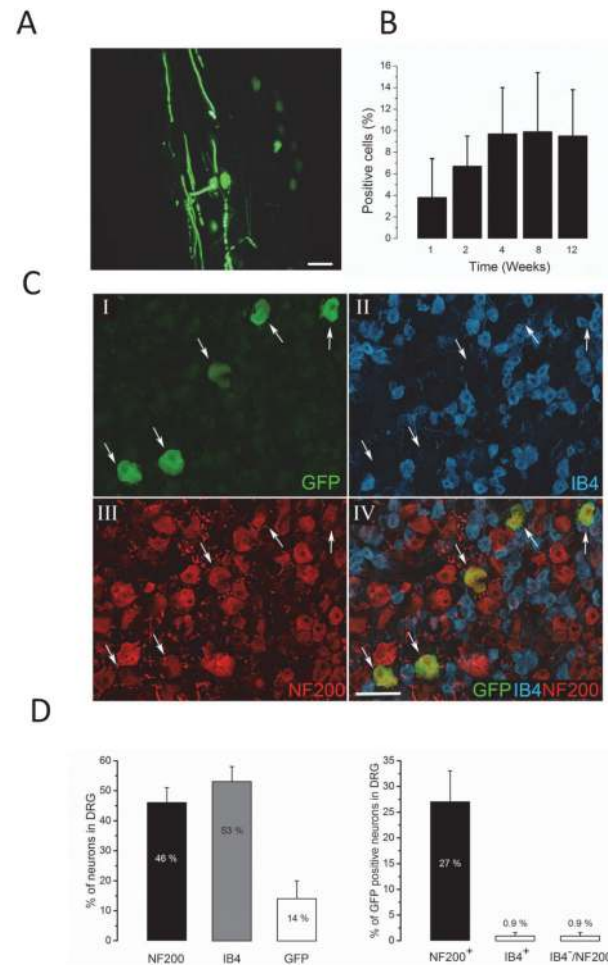




**Figure 1.**

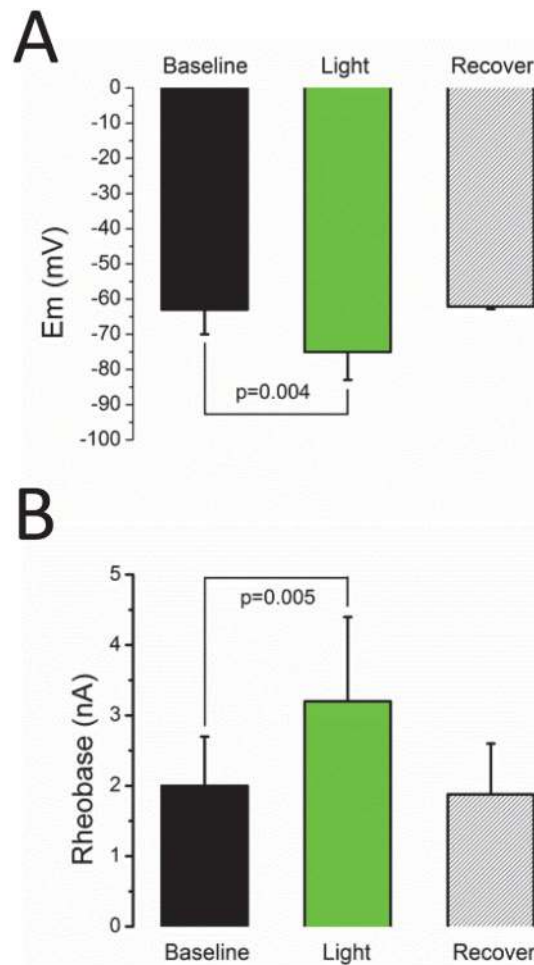
ArchT modulation of peripheral neuron activity.

A: The gene for the protein pump ArchT is fused to GFP for detection and is used with a ubiquitous and non-selective promoter. The gene is packaged in adeno-associated virus-type 8 (AAV8) for cell insertion and expression of the ArchT. B: Although the promoter and AAV8 are thought to be non-selective, the ArchT is expressed (>98%) and functional (100%) in specific cells, in this case fast conducting (A- $\delta$ , myelinated) high threshold mechanoreceptors (AHTMR), as determined by electrophysiological characterization of the peripheral neuron and its receptive field. It was not expressed (by immunohistochemistry (<2%) and/or non-functional (electrophysiology (0%)) in myelinated, fast conducting (A-type fiber), low-threshold mechanoreceptors (LTMR) and the unmyelinated, slow-conducting (C-type fiber) high-threshold mechanoreceptors (CHTMR). The proton pump ArchT is expressed throughout the membrane of the neuron. C: Light activation, through the interaction of the cofactor retinal, results in protons being pumped from the intracellular to the extracellular space. This hyperpolarizes the neuron and reduces excitability and/or inhibits neuronal activity.



**Figure 2. Neuronal expression of ArchT after intrathecal administration**

(a-d) AAV8-CAG-ArchT-GFP viral particles were administered *in vivo* by intrathecal injection for all experiments. (a) Expression of ArchT-GFP in DRG soma and in axons and dendrites from the L4 nerve roots was consistent, reproducible, and easily visualized. This photo demonstrates nascent epifluorescence of GFP in fresh frozen sections of DRG (no antibody enhancement). (b) Expression was quantified in fresh sections without the use of antibody enhancement, reaching a maximum expression 3-4 weeks after administration. This level of expression was maintained for at least 12 weeks (N=4 animals at each time point). (c) The ArchT was selectively transduced in myelinated neurons (c: Panel I, GFP alone; Panel II, IB4 alone; Panel III, NF200 alone; Panel IV, merge of all three). This is seen with co-localization of the NF200/GFP at 4 weeks after injection (arrows pointing to GFP positive cells with NF200 co-labelled; no IB4 positive cell expressing GFP). (d) Quantification of IB4, NF200 and GFP labelling. GFP co-labelled with IB4 was present in <1% of neurons. In contrast, >98% of GFP positive neurons were NF200 positive and 27% of NF200 positive neurons were co-labelled with GFP.

**Figure 3.**

In vitro functional activity of ArchT.

(a,b) *In vitro* responses of neurons were measured by removing L4 DRG 3-4 weeks after injection and single cell intracellular recordings performed in cells expressing GFP a(n=12 neurons from 12 DRG from 12 animals). Resting membrane potential ( $E_m$ ) became hyperpolarized (a) ( $p < 0.05$ ) and rheobase was increased (b) ( $p < 0.05$ ) after 2-min of exposure to 480-550 nm light (Irradiance= 0.013 mW/mm<sup>2</sup>).

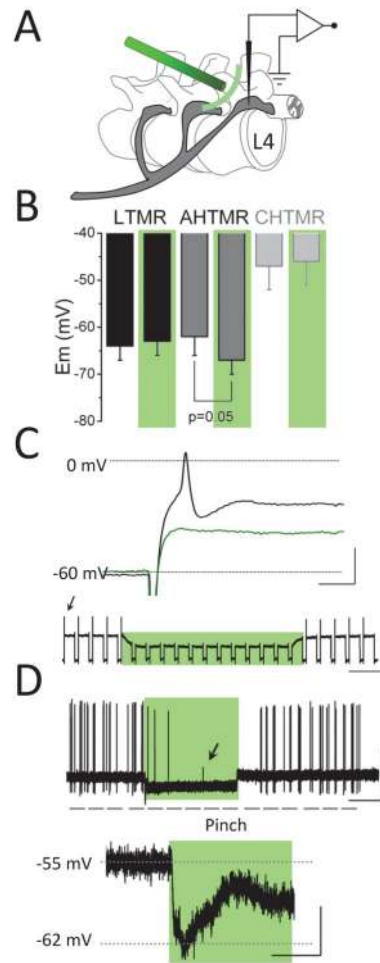


**Figure 4.**

In vivo neuronal subtype specific functional activity of ArchT.

(a-d) *In vivo* electrophysiology of DRG was performed to assess the effects of optical activation in subtype specific neurons with light activation at the soma (a). Only myelinated, fast conducting high threshold mechanoreceptors (AHTMR) were affected by light (532 nm wavelength (Irradiance 0.03-0.1 mW/mm<sup>2</sup>)) with resulting hyperpolarization while the myelinated, low threshold mechanoreceptors (LTMR) and the unmyelinated, slow conducting high threshold mechanoreceptors (CHTMR) were unchanged (b) (n=49 neurons (maximum one neuron of each type per animal) from 20 animals; 15 AHTMR, 19 LTMR, 15 CHTMR). Green shading represents light administration. (c) A representative AHTMR neuronal response to threshold electrical activation from a somatic intracellular recording pipette (rheobase) and inhibition of the action potential (AP) with somatic optical activation are shown (c: scale bar=Upper trace: 20 ms/20 mV; Lower trace: Pulses: 500 ms, 1.2 nA, 0.5 Hz, scale bar=1 sec/40 mV). This inhibition at threshold could only be produced in the AHTMR population. (d) Peripherally generated AP in a nerve with a receptive field (RF) in the paw was recorded from the intracellular pipette in the soma of the DRG. Suprathreshold von Frey stimulus was used in the plantar surface RF of the paw to elicit the AP and during the stimulus laser light at a wavelength of 532 nm at the DRG resulted in elimination of AP with return after the light was eliminated. The arrow shows an electrotonically propagated

AP. The higher magnification of the baseline  $E_m$  shows the speed of the change in  $E_m$  of the cell with the illumination of the soma with an almost instantaneous 7 mV hyperpolarization of the soma. Only AHTMR neurons could be inhibited at the soma (15/15 AHTMR, 0/19 LTMR, 0/15 CHTMR) ( $p < 0.001$ ).

Author Manuscript

Author Manuscript

Author Manuscript

Author Manuscript

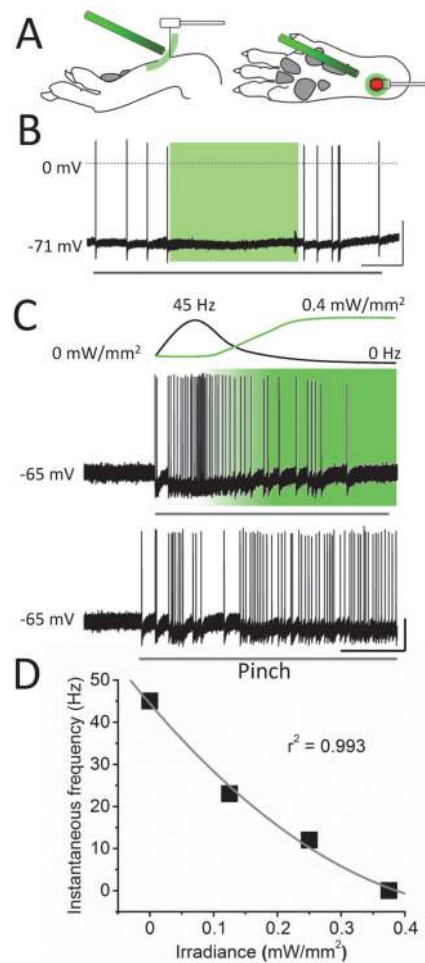


**Figure 5.**

Transcutaneous light activates ArchT AHTMR in paw.

(a-d) *In vivo* electrophysiology at the soma of the DRG was utilized to test transcutaneous efficacy of light inhibition in the RF (Irradiance 0.15-0.34 mW/mm<sup>2</sup>) (a). Only AHTMR neurons could be inhibited transcutaneously (n= 23 neurons (maximum one neuron of each type per animal) from 11 animals; 8/8 AHTMR, 0/8 LTMR, 0/7 CHTMR) (p < 0.0001). (a) A representative AHTMR at threshold (b: scale bar=0.5 sec/20 mV) and at suprathreshold demonstrates inhibition of AP generation (c: scale bar=20 ms/20mv). The response to supathreshold stimulus is also presented underneath in the absence of light (c). A dose response of instantaneous frequency of the neuronal AP responses to light intensity is also presented (d).



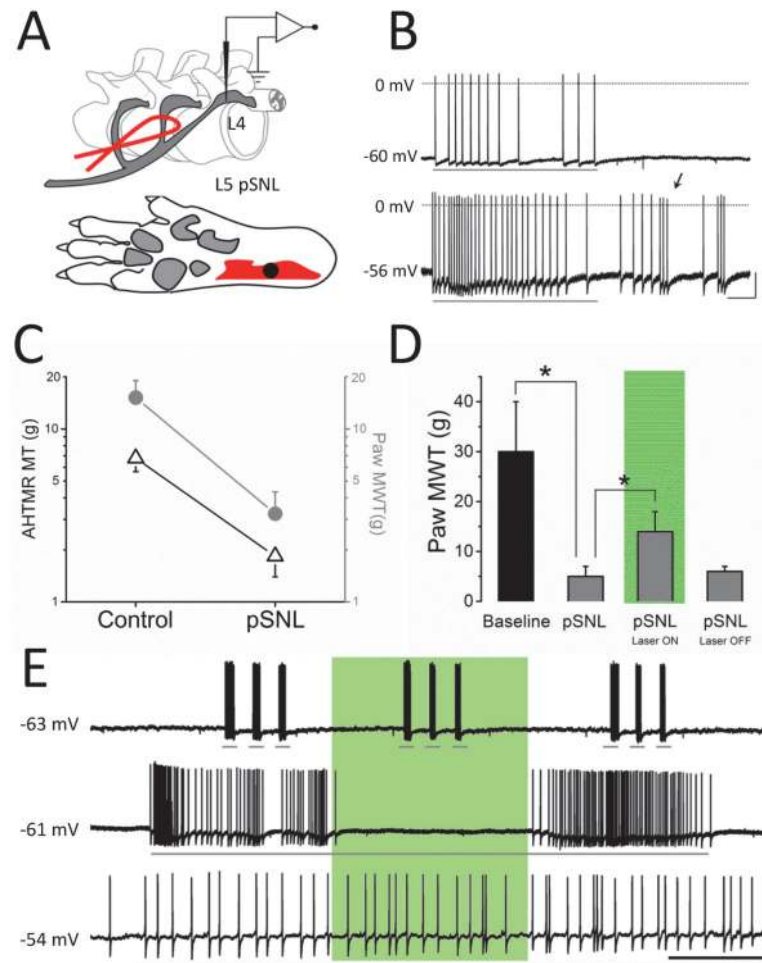


**Figure 6.**

Inhibition of nerve injury induced neuronal hyperexcitability using transcutaneous light administration.

(a-e) Partial sciatic nerve ligation (a) (partial ligation of the L5 nerve root (pSNL)) was performed and the effects of neuronal responses to stimulation with and without light were assessed. The neuronal RF was mapped with an increase in receptive field (RF) size after pSNL compared to control (a: paw with black shading control RF size; red shading RF size after pSNL) and response testing of light administration (green shading) was performed within the neuron RF. Representative tracings of AHTMR from sham with a threshold of 10 g (panel b, top tracing) and from a neuron from an animal 2 weeks after pSNL with a threshold of 0.6 g (panel b, bottom tracing) (b: scale bar=2 sec/20 mV). Hyperexcitability is noted by increased instantaneous frequency response at threshold and afterdischarges (arrow, panel b, bottom tracing) (not present in normal or sham AHTMR neurons). Bar underneath the AP responses is the duration of the threshold von Frey filament stimulus. The pSNL resulted in decreased mechanical thresholds (MT) tested by RF stimulation on the glabrous skin of the paw using von Frey filaments and measured in isolated AHTMR neurons *in vivo* using intracellular electrophysiology at the soma of L4 DRG neurons (open triangles, left axis, panel c) (n=28 AHTMR neurons from 23 animals (one cell per animal);

11 pSNL and 17 sham/control). Mechanical withdrawal thresholds (MWT) in awake freely mobile animals were also reduced after pSNL compared to sham controls and these MWT (gray circles, right axis, panel c) were reduced consistent with the reduction in MT of isolated AHTMR neurons from L4 measured electrophysiologically by threshold AP activity at the soma (open triangles, left axis, panel c). (d) Hyperalgesia is present with a reduction in MWT 2 weeks after pSNL compared to baseline and transcutaneous light administration for on the paw of freely moving animal 2 min prior to von Frey threshold testing increased MWT (reduced hyperalgesia (n= 8 animals) (\*p < 0.05). This returned to baseline 5 min after the light was turned off. (e) Effects of transcutaneous light in the RF of LTMR (top panel), AHTMR (middle panel), and CHTMR (bottom panel) on neuronal RF neuronal responses (e: scale bar=4 sec/20 mV). Green shading represents light administration. Only AHTMR activity could be inhibited by light (n=9/9 cells from 9 animals). No CHTMR (0/6) and no LTMR (0/7) neuron was inhibited (p<0.05).